189

SATELLITE & MESOMETEOROLOGY
RESEARCH PROJECT

Department of the Geophysical Sciences
The University of Chicago

IN SEARCH OF MESOSCALE WIND FIELDS IN LANDFALLING HURRICANES

T. Theodore Fujita

(For Postprint Volume of Invited Papers)
13th Technical Conference on
Hurricanes and Tropical Meteorology
American Meteorological Society
December 1-5, 1980 MIAMI BEACH, FLORIDA

SMRP Research Paper

IN SEARCH OF MESOSCALE WIND FIELDS IN LANDFALLING HURRICANES

T. Theodore Fujita

The University of Chicago
Chicago, Illinois

ABSTRACT

During the past two decades, Fujita worked with the three-generation research laboratories, NHRP, NHRL, and NHEML in search of the storm damage related to the mesoscale structure of hurricanes. Historical survey data of three hurricanes, Camille (1969), Celia (1970), and Frederic (1979), were put together for reconstructing the structure of these landfalling hurricanes.

It was found that the shape of radar eyes change periodically from circles to ellipses while their long axes rotate cyclonically. There were localized areas of high winds inside the overall areas of Camille and Frederic, which are suspected to be associated with downbursts in hurricanes. The downburst in Celia came from westerly directions where the eye-wall convection was affected by dry continental air.

1. INTRODUCTION

Because of the vast areas of wind damage by landfalling hurricanes, aerial photography and mapping had long been limited to the coastal zone where storm surge and waves leave behind the most spectacular damage.

Fujita and his associates at the University of Chicago have performed damage surveys of tornadoes, long and short, wide and narrow, weak and intense, etc. The aerial coverage of such damage was only a fraction of a typical hurricane area.

The first case of an organized tornado survey occurred after the Palm Sunday tornadoes of April 11, 1965. This experience of extensive aerial photography, thus performed, made it possible to undertake aerial photography and mapping of hurricane damage.

The first chance occurred when hurricane Camille crossed the Gulf Coast on August 17, 1969. A 50 mi x 100 mi or 5,000 sq mi area was surveyed from a low-flying Cessna 172.

The second storm, hurricane Celia moved inland from north of Corpus Christi. The damage pattern of this hurricane was analyzed based on 9" x 9" color photos by NASA and 35-mm pictures by Dr. R. H. Simpson from a low-flying helicopter.

Finally, hurricane Frederic damage was surveyed by Fujita, Wakimoto, and Stiegler of the University of Chicago, obtaining over 3,000 vectors of damaging winds.

These results, along with the mapping of the storm surge, will assist hurricane forecasters, the hurricane strike program in particular, in predicting the areal extent and nature of hurricane winds during landfalling and post-landing phases of destructive hurricanes.

This report will elaborate on the historical aspects of these hurricanes emphasizing their radar echoes, central pressure, and mesoscale damage patterns (Figure 1).

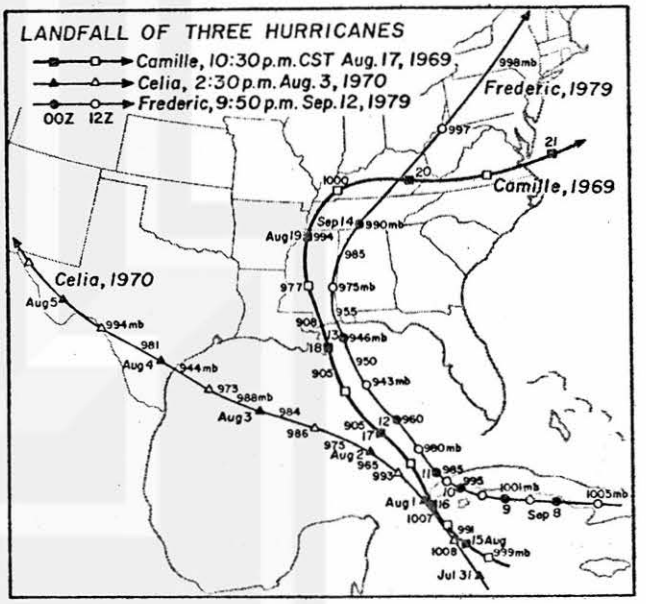

Figure 1. Paths of three landfalling hurricanes, Camille, Celia, and Frederic. Their landfalling central pressures were 908 mb, 944 mb, and 950 mb, respectively.

2. HURRICANE CAMILLE (AUGUST 1969)

Camille was a small but intense hurricane with its minimum, prelanding pressure of 901 mb. At Bay St. Louis, the landing site, the minimum pressure of 909 mb was measured. Thereafter, the central pressure increased rapidly as the hurricane center moved toward Memphis, Tennessee.

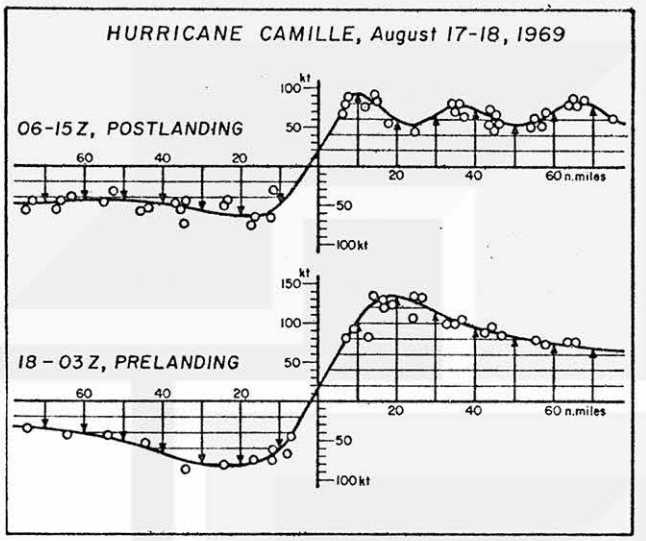

Figure 2. Velocities of echoes on the east and west sectors of Camille during the 6-hour periods, postlanding (upper) and prelanding (lower) time.

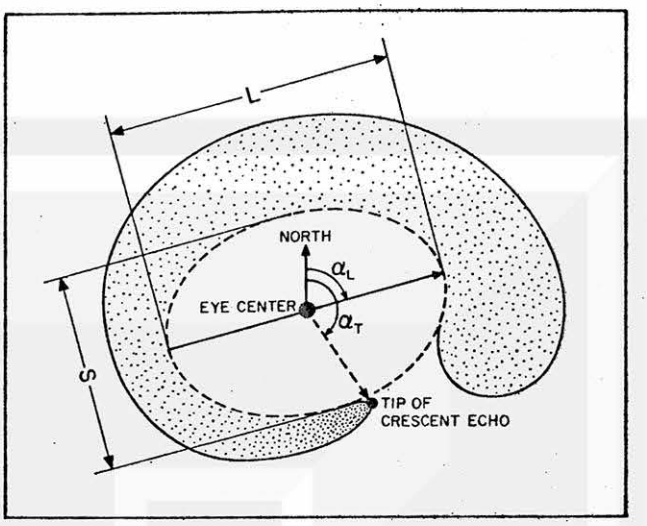

Figure 3. Definition of L, long axis, S, short axis, and the azimuths of the long axis and the tip of the crescent echo.

The radar-echo velocities plotted as a function of the distance from the center shows that the echo motion on the east side of the path was as fast as 140 kt during the prelanding period, 18 - 03 GMT, August 17-18. Between 06 and 15 GMT when the storm center was in southern Mississippi, the maximum echo motion slowed down to 90 kt. There were several rain bands of high-speed echo motion on the east side of the storm center (Figure 2).

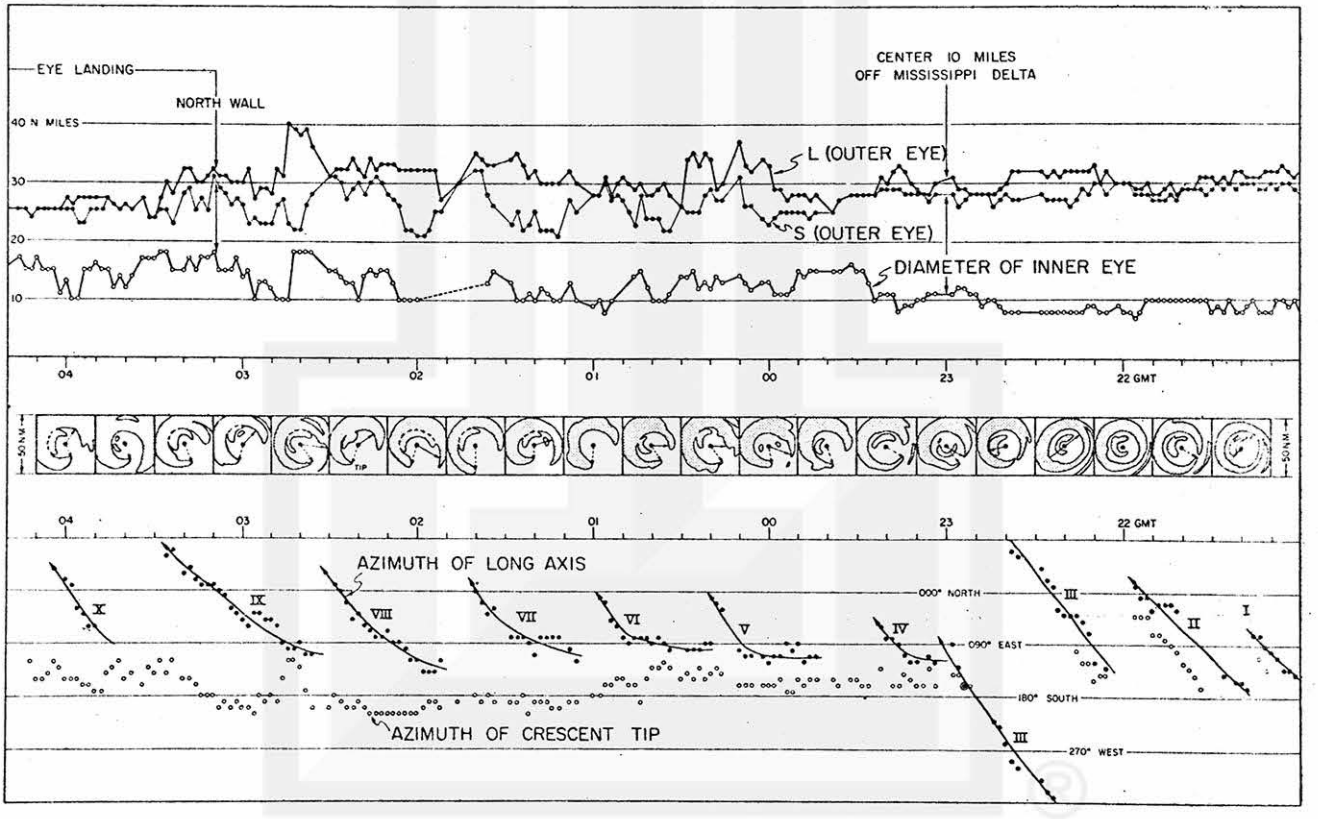

Figure 4. Variation of long and short axes (L and S) of the elliptic eye of Camille. This figure also includes the diameter of inner eye, shape of eyewall echoes, and azimuths of the long axis and the crescent tip.

The overall shape of the eye-wall echo was characterized by an "elliptic eye-wall" and the "tip of the crescent echo". The azimuths of the long axis and that of the tip of the crescent echo were measured. L denotes the long axis and S, the short axis (Figure 3).

Figure 4 shows the time variations of L, S, and azimuths of the long axis and crescent tip. Between 21 GMT on the 17th and 04 GMT on the 18th an inner eye was visible in radar pictures. The diameter of the inner eye, approximated as a circle, was also plotted in the figure.

A rather interesting thing is the periodic variation of the eccentricity of the eye approximated as an ellipse. The eccentricity oscillated between 0.0 and 0.9 with its mean period of 49 minutes (max. 73 min and min. 28 min). As expected, there were high-frequency variations due in part to a measuring error. During periods IV, VIII, and IX, however, a dip is seen in the middle of each period (Figure 5).

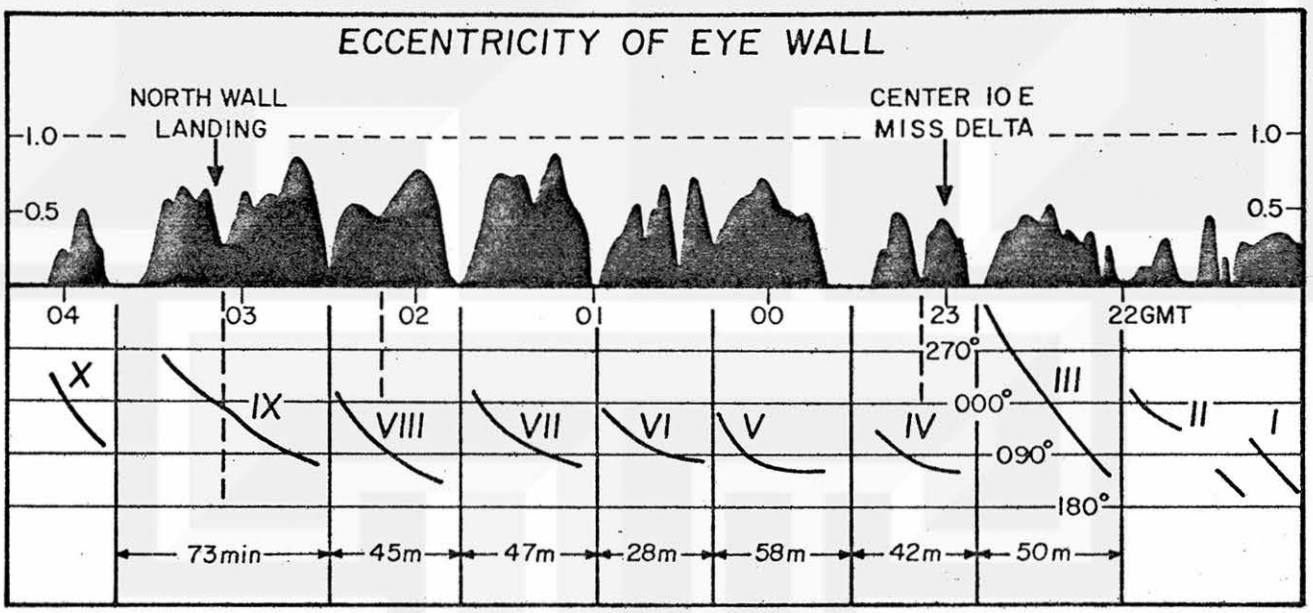

Figure 5. Periodic change in the eccentricity of the elliptic eye computed from L and S in Figure 4. The variation of eccentricity is accompanied by the rotation of the long axis.

The long axis rotated cyclonically in each period from approximately 120° azimuth to 000° and further. The azimuth of the crescent tip (Figure 4) remained, more or less, at 150°. A combination of the variations of eccentricity, azimuths of the long axis and crescent tip now permits us to describe the evolution of the eye wall during an oscillation period (Figure 6).

The mechanism of this evolution is not clear at this time. It is likely, however, that an azimuthal variation of the inflow into the eye wall is one of the causes of this phenomenon. A strong flow from the south, entering the east wall of the eye, could overshoot toward the north and then west, resulting in an increase in eccentricity and also, in the rotation of the axis. At stage 4 in Figure 6, the eye will return to its original semicircular shape.

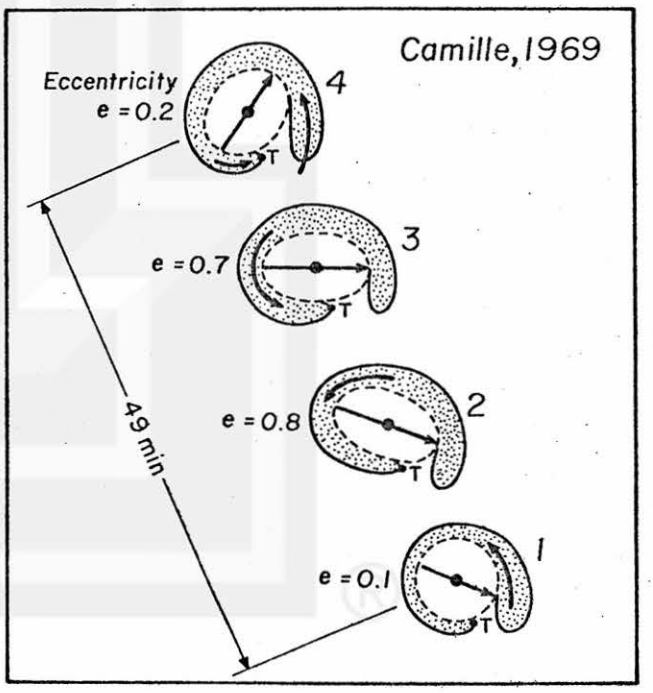

Figure 6. Schematic evolution of the eye wall of hurricane Camille characterized by the rotation of the long axis while the tip of the crescent echo to the south of the eye remains at the same location relative to the hurricane center.

The strong southerly flow does not have to oscillate periodically. It is likely to be a steady-state of high-speed inflow. The periodic oscillation could easily be caused by the evolution of the eye wall triggered by the forcing function of the exitation.

Do similar oscillations occur over the ocean? The answer to this question is "yes", provided that the inflow structure is not axial symmetric. Near the coastal regions, however, the assymmetry will become larger, causing a significant oscillation during the landfalling period.

After the landfall, the eye wall began disintegrating while the maximum echo speed dropped considerably. Figure 7 depicts the echo motions at 12 GMT when the circulation center was just to the south of Jackson, Mississippi. Practically no damage on the ground was sighted from the air in and around Jackson.

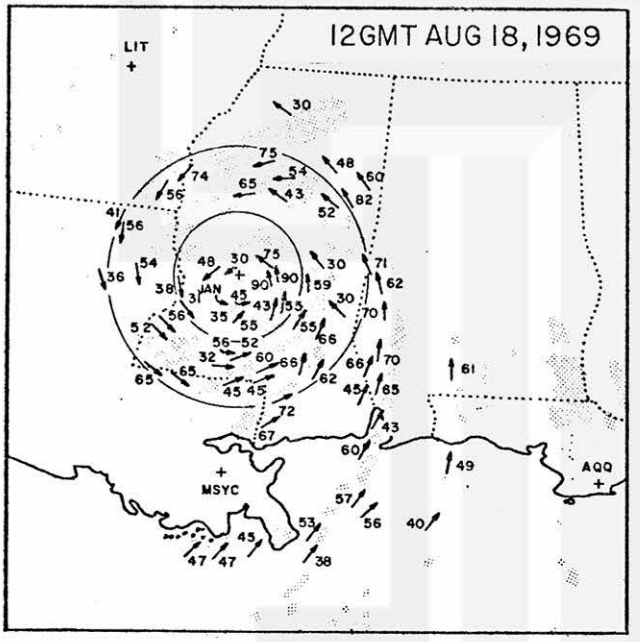

Figure 7. Velocities of radar echoes at 12 GMT when the hurricane center was just to the south of Jackson, Mississippi.

Mesoscale damage patterns mapped from a low-flying Cessna 172 are shown in Figure 8. The initial mapping was performed by assigning the F-scale values during the Cessna flight. They were later converted into the windspeed contours at 25 mph intervals.

Determined from the air is the time sequence of damage events, the inital and the subsequent damage. In forested areas, we can easily determine the order of the wind damage based on the overlaying/underlaying configuration of tree falls.

On both sides of the hurricane center, the initial tree falls were from the east through northeast. The subsequent falls were predominantly from the southeast, suggesting that these high winds occurred (1) when the weakening hurricane was approaching and (2) when the center was passing nearby. In other words, hurricane Camille maintained its strong core circulation until it passed Poplarville, Mississippi.

There were a number of high-wind streaks to the west of the center. These streaks, 3 to 5 mi wide and 5 to 10 mi long could be hurricane-embedded downbursts which had not been known in 1969. Fujita first identified the "downburst" early in 1976.

Hurricane Camille was characterized by both small core and strong winds. The eye center passed over Bay St. Louis, Mississippi, moving north-northeast. The width of the estimated 125 mph and stronger winds were only about 9 to 12 mi extending as far as 40 mi inland. The tree damage inside this area was rated as F2 (113 - 157 mph). Most pecan trees were uprooted, pine trees were snapped 5 to 10 ft above the ground, and high-tension towers were damaged.

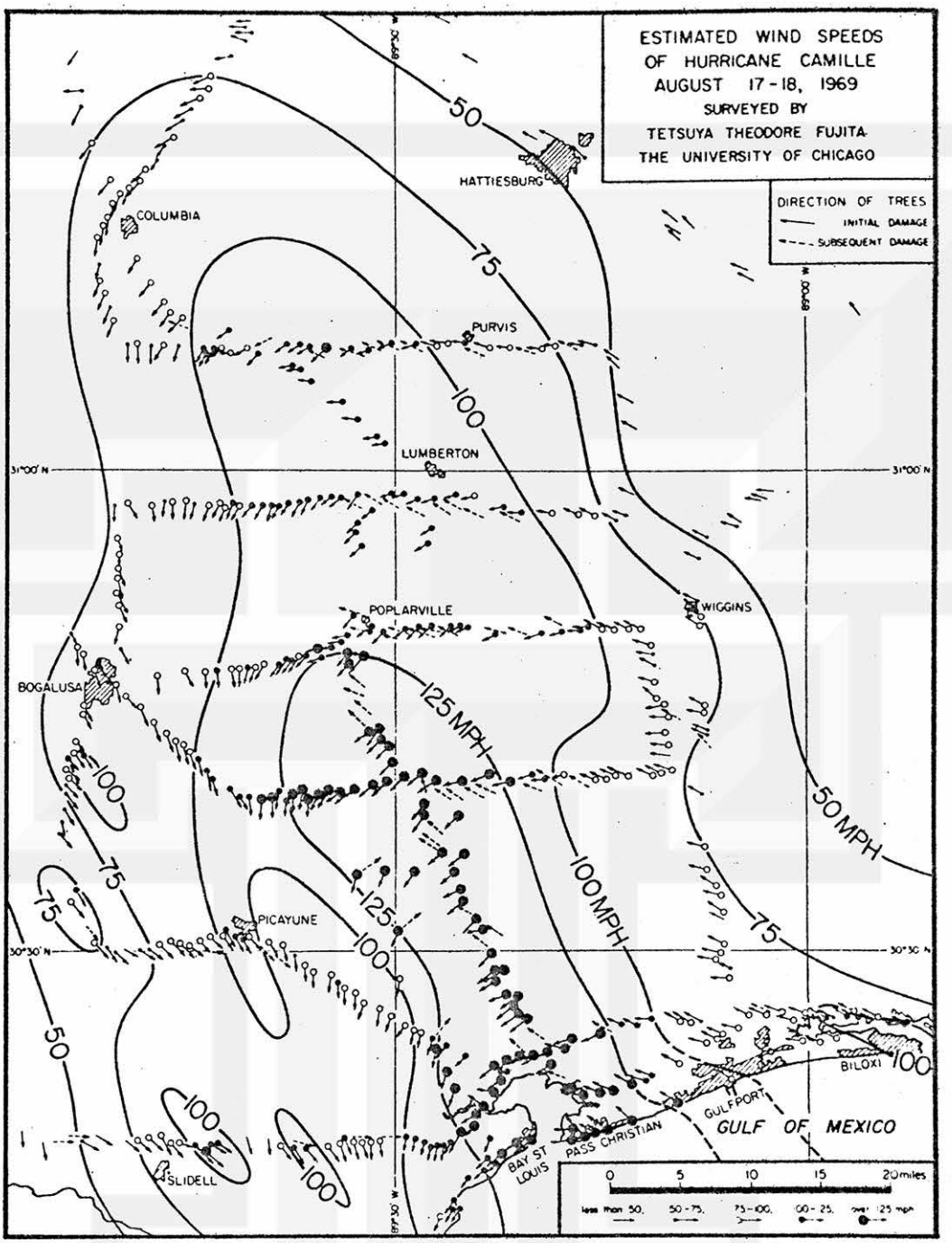

Figure 8. Patterns of estimated windspeeds of hurricane Camille depicted by isotachs at 25 mph intervals. Aerial mapping was made by Fujita from a Cessna 172 flying between 1,000 and 1,500 ft AGL. The high wind core extended 40 miles inland to near Poplarville, Mississippi.

3. HURRICANE CELIA (AUGUST 1970)

Hurricane Celia moved from the western tip of Cuba to Corpus Christi across the central Gulf, taking about 3 days. The central pressure reached a minimum of 965 mb two days in advance of the landfall. Then it increased to 988 mb.

During the 24-hour period prior to the landfall, the central pressure kept dropping steadily reaching 944 mb at 2130 GMT on August 3, the landfall time. Thereafter, the central pressure increased rapidly (Figure 1).

The path of Celia and her eye-wall circulation are presented in Figure 9. The landfall took place to the south of Aransas Pass, Texas, 15 mi to the northeast of Corpus Christi.

The eye-wall echo was in elliptic shape with its long axis oriented in an east-to-west direction (Figure 9).

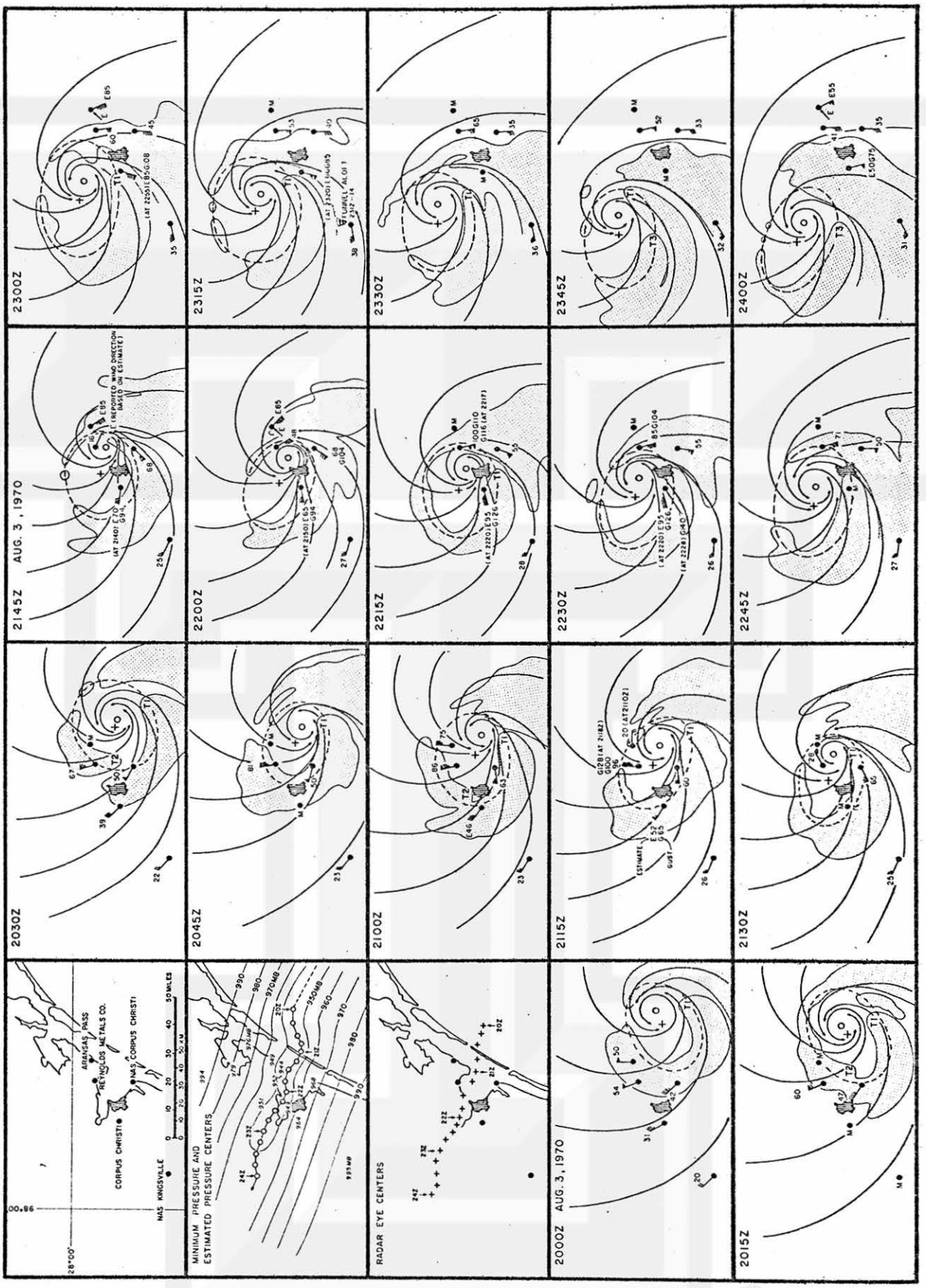

Figure 9. Shape of the eye of hurricane Celia depicted by combining the Galveston and Brownsville radar pictures. Apparently, the geometric centers of the radar eye and the pressure field were separated by up to 10 miles.

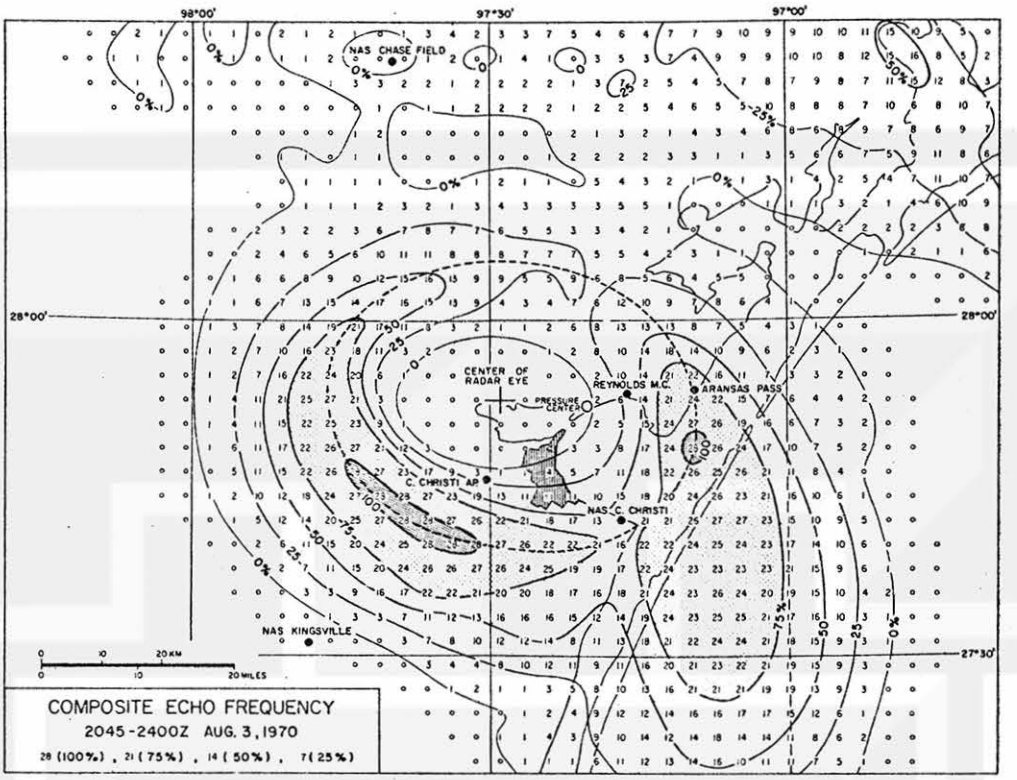

Figure 10. Percent frequencies of the presence of radar echoes around Celia's eye. Note that there were always echoes to the southwest and east-southeast of the eye center.

The eye wall was not surrounded continuously by radar echoes. Instead, there were echo-free gaps often visible to the northeast and to the southeast of the center. For the purpose of determining the frequencies of echoes in and around Celia's eye, composite echo frequencies (in %) were obtained relative to the eye center for a 3 hour and 15 min period between 2045 and 2400 GMT, August 3, 1970. The composite frequency pattern was then superimposed upon the hurricane position at 2230 GMT (Figure 10).

There were radar echoes 20 mi to the east-southeast and 15 mi to the southeast of the eye center 100% of the time. On the other hand, the northeast eye wall was open (6% echo) most of the time.

The pressure center estimated from barograph traces was located 8 mi to the east of the eye center, suggesting that the surface pressure around the eye-wall echoes is not constant. Namely, the pressure on the west wall is higher than that on the east wall.

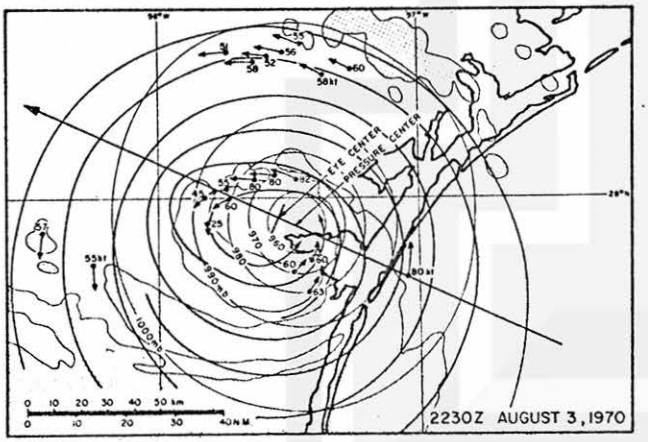

Figure 11. Eccentric eye wall of hurricane Celia superimposed upon the surface-pressure field obtained from barograph traces. Note that speeds decrease as eye-wall echoes move westward against the pressure gradient.

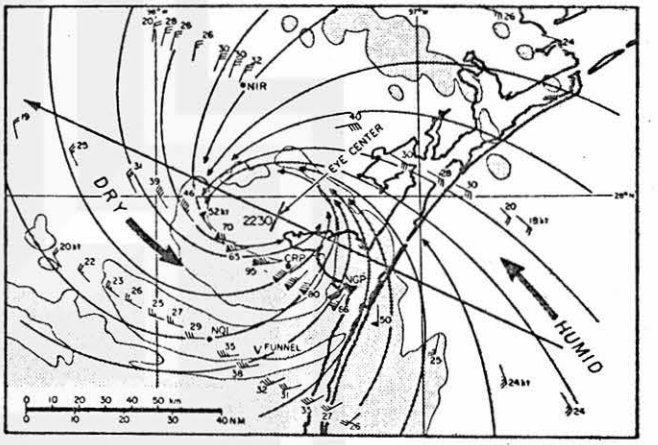

Figure 12. Mesoanalysis of surface winds of Celia at 2230 GMT August 3, 1970. Against all expectations, the stronger winds are seen on the left side of this travelling hurricane.

Figure 11 presents the eye-wall and surface-pressure relationship along with the computed echo velocities. The pressure center is located near the eastern focus of the eye ellipse suggesting geometrically that the eye-wall echoes are distributed along a hypothetical orbit around the astronomical body at the pressure center.

The 82 kt velocity of the echo to the north of the pressure center appears to decrease toward the west, reaching only 25 kt at the western eye wall where the pressure is the highest. Are radar echoes playing a see-saw game as they orbit around the pressure center? There is no satisfactory answer to this question at this time.

A mesoanalysis of surface winds at the same time of Figure 11 reveals the existence of a significant convergence of the eastern sector of the eye wall (Figure 12).

For the purpose of evaluating the minute-by-minute variation of the long axis (L) and the short axis (S) of Celia, both Galveston and Brownsville radars, scanning from the opposite directions, were used. Plotted values revealed that the pattern of variations is very similar to that of hurricane Camille presented earlier. Both L and S and their differences vary periodically along with the rotation of the long axis. The azimuth of the tip of the crescent echo remained approximately 120° (Figure 13).

The basic period of the variation of the eccentricity is 66 min which is 35% longer than 49 min period of hurricane Camille. Interestingly, however, every cycle of Celia is characterized by the half-period oscillations which are coupled with the long-axis rotation (Figure 14).

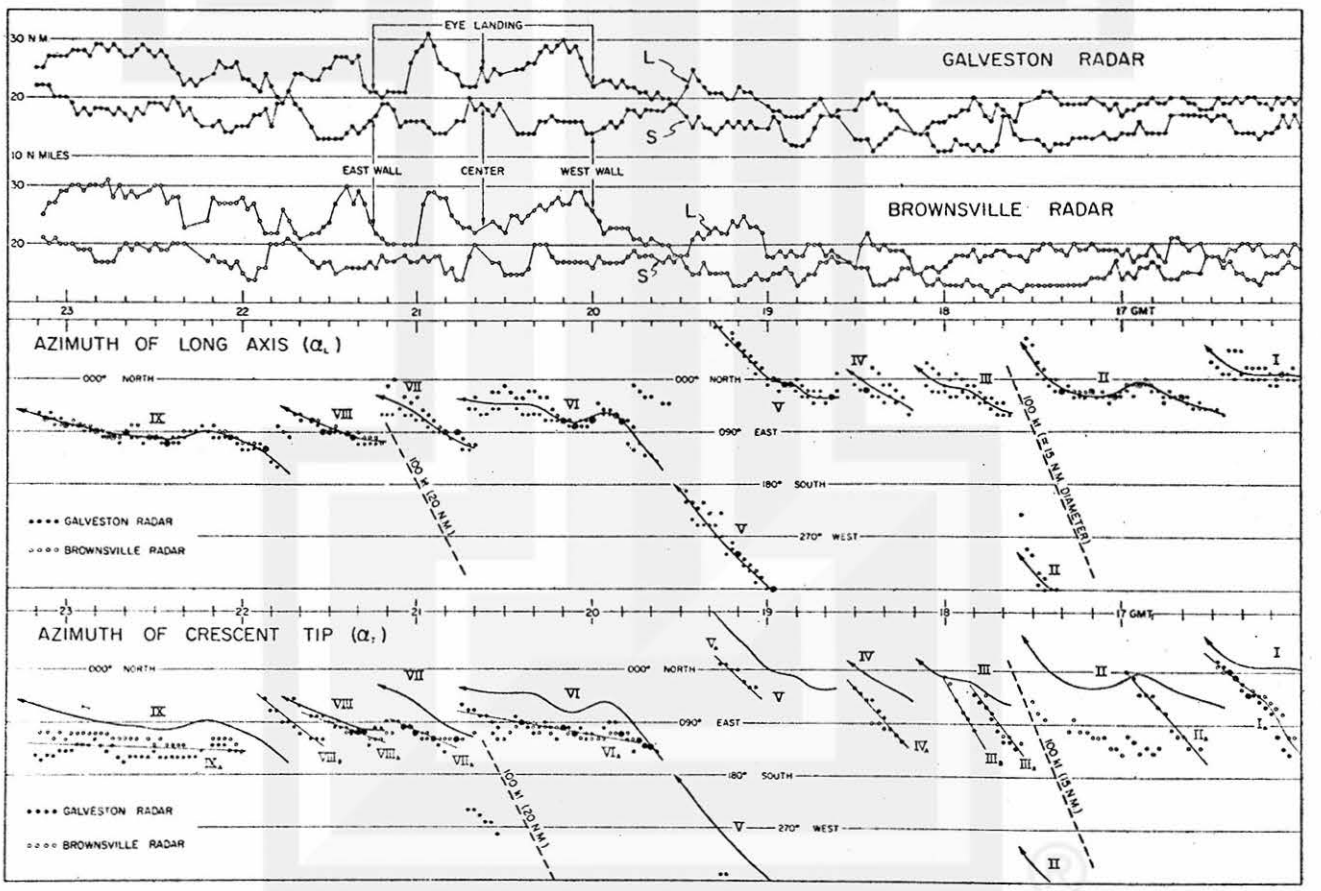

Figure 13. Periodic variations of L, the long axis, S, the short axis, and the azimuths of the long axis and the tip of the crescent echo.

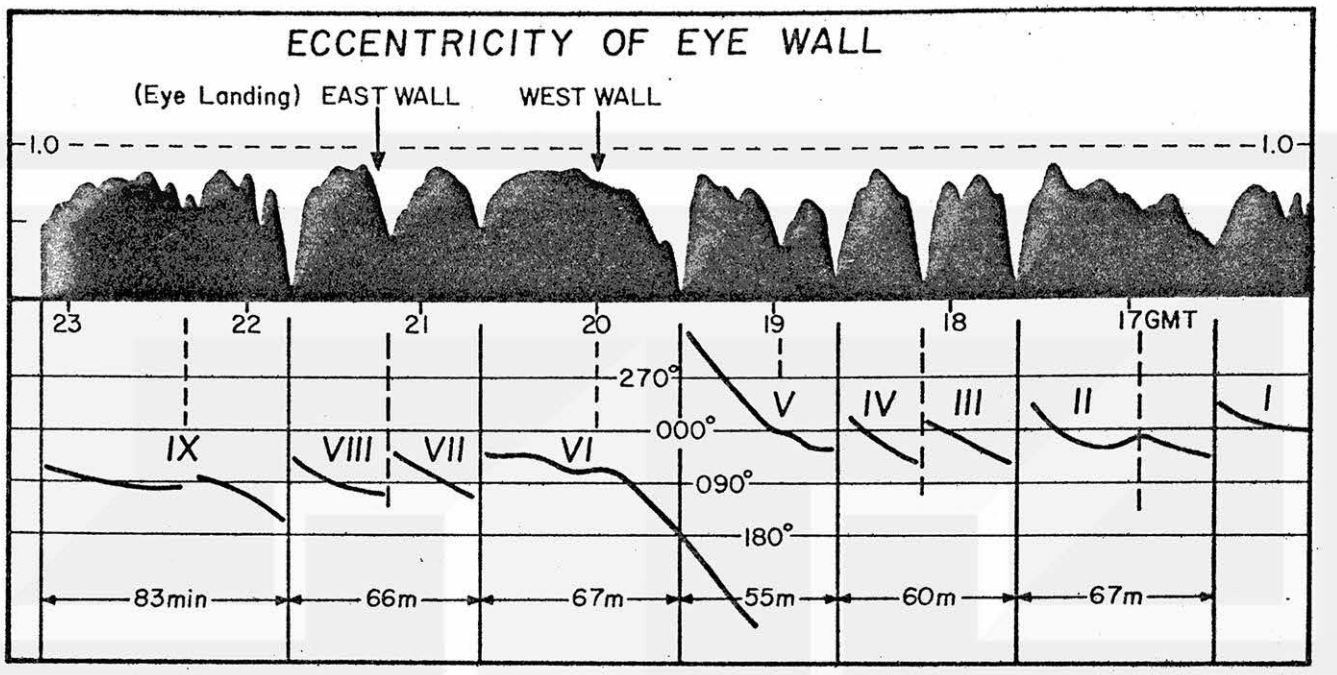

Figure 14. Periodic variation of the eccentricity of the eye-wall ellipse which is coupled with the rotation of the long axis of the ellipse. The half-period variations are seen in every basic period with its mean period of 66 minutes.

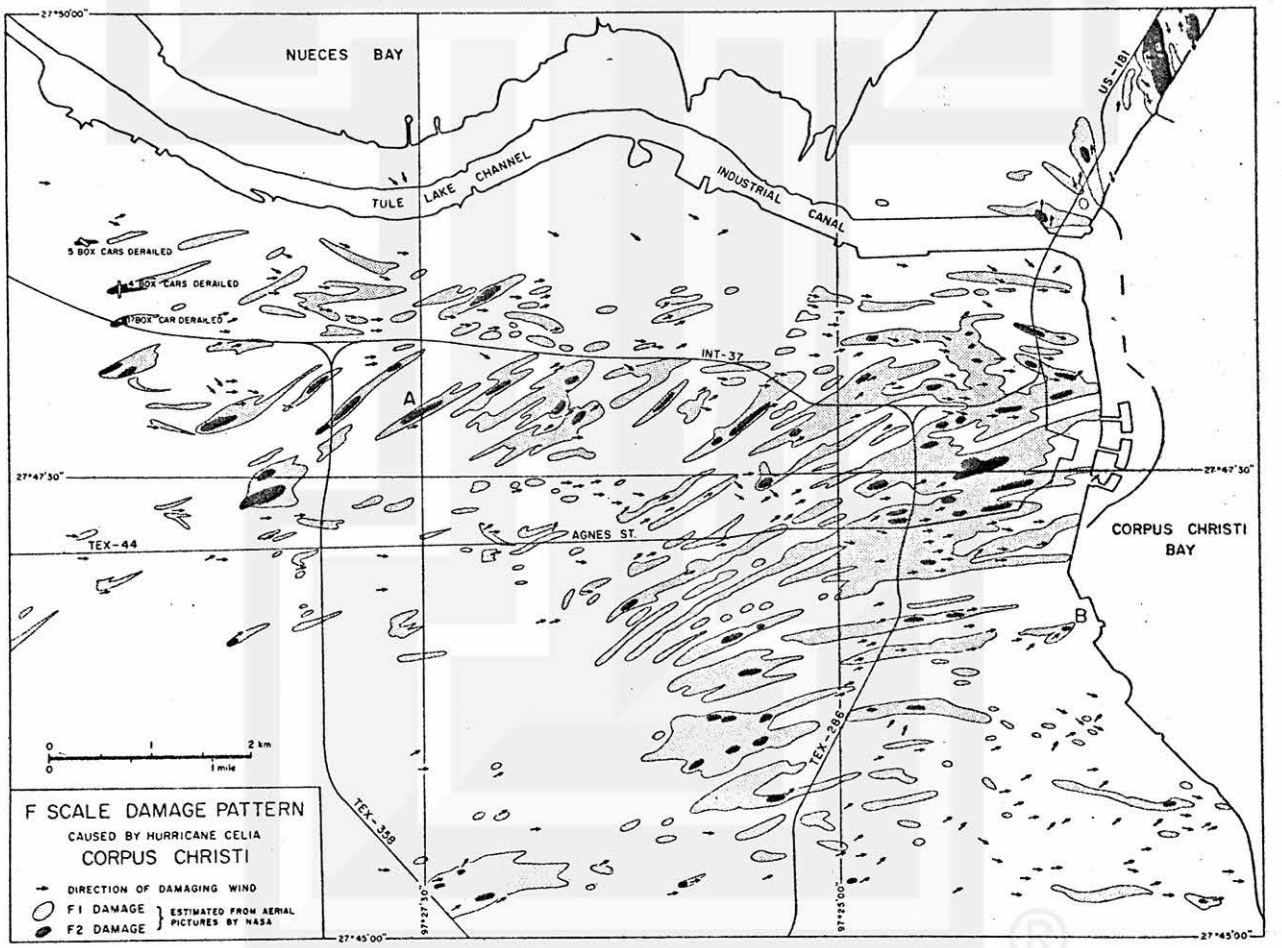

Figure 15. F-scale damage patterns over Corpus Christi, Texas. Arrows indicate directions of uprooted trees and strewn debris.

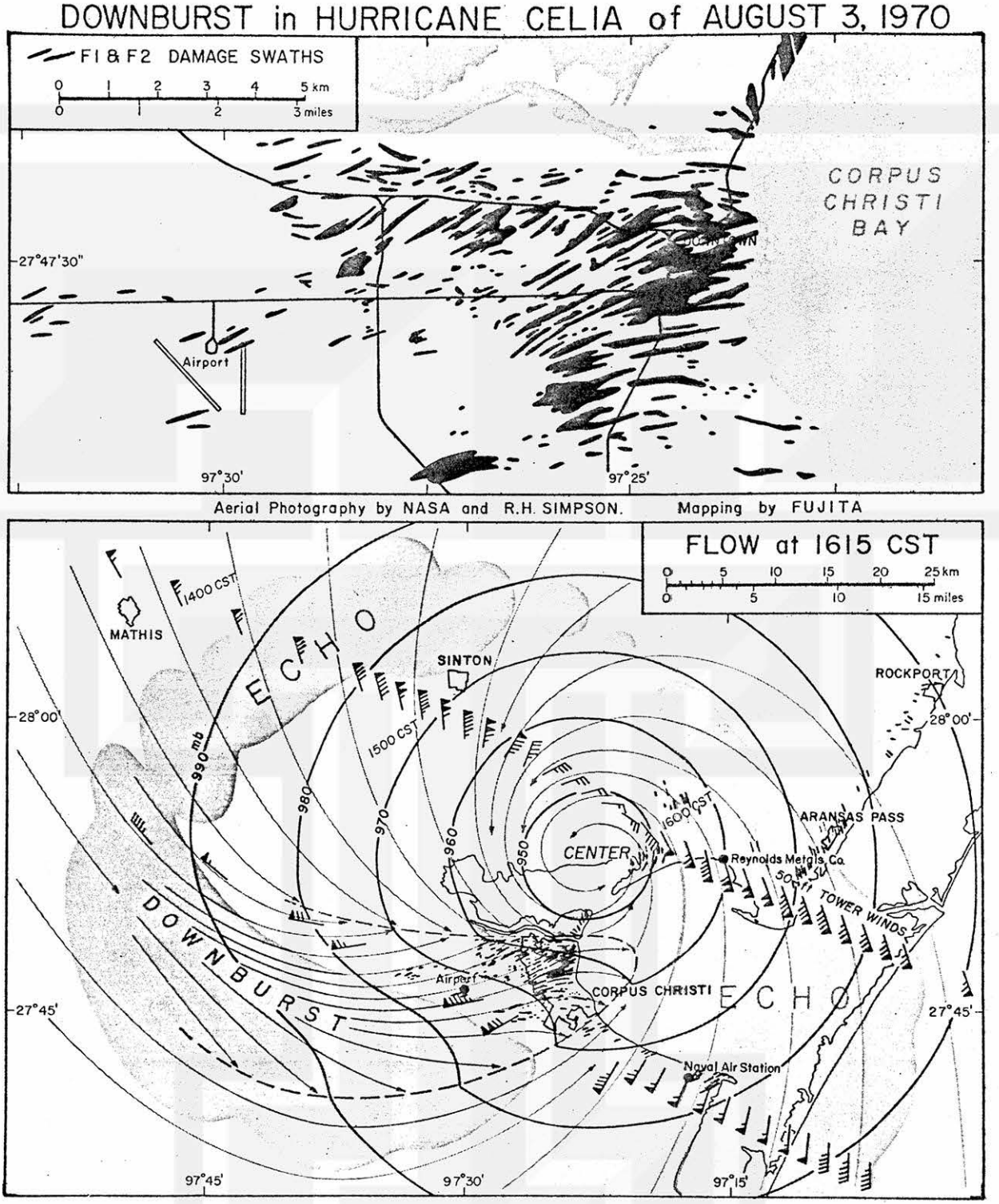

Figure 16. Two-scale maps of Celia's damage. F1 and F2 damage swaths in Corpus Christi (above) and damage swaths superimposed upon isobars and radar echoes at 2215 GMT (4:15 p.m. CST) on August 3, 1970.

As was reported initially by Dr. R. H. Simpson, there was severe wind damage in Corpus Christi located on the left-hand side of the Celia's path. The detailed mapping of the damage patterns clearly shows a number of interesting features (Figures 15, 16, and 17).

The unusual direction of strong winds at Corpus Christi may be explained as downburst winds originating in the southwest eye wall where large echoes were located 100% of the time. Thunder was heard at the airport from the direction of the large-echo eye wall which displayed characteristics of a mixture of the eye-wall and squall-line echoes.

Dew-point (temperature) spread at 00 GMT August 4, 1970 shows that hurricane Celia from the Gulf plunged into the dry area dominating the western two-thirds of Texas. 20°F spread is seen across the central part of Texas (Figure 18).

It is plausible that the eye wall, being exposed on its west and southwest sides to dry continental air, turned into thunderstorms which induced strong downflow. The downflow, after reaching the surface, could be accelerated by a 20 to 30 mb pressure gradient of hurricane pressure field in inducing the strong winds from west-southwest over the city of Corpus Christi.

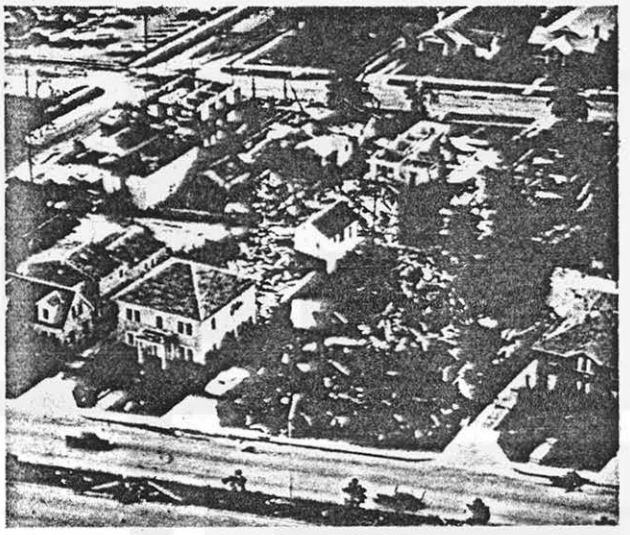

Figure 17. A typical damage swath in Corpus Christi, Texas. Courtesy of Dr. R. H. Simpson.

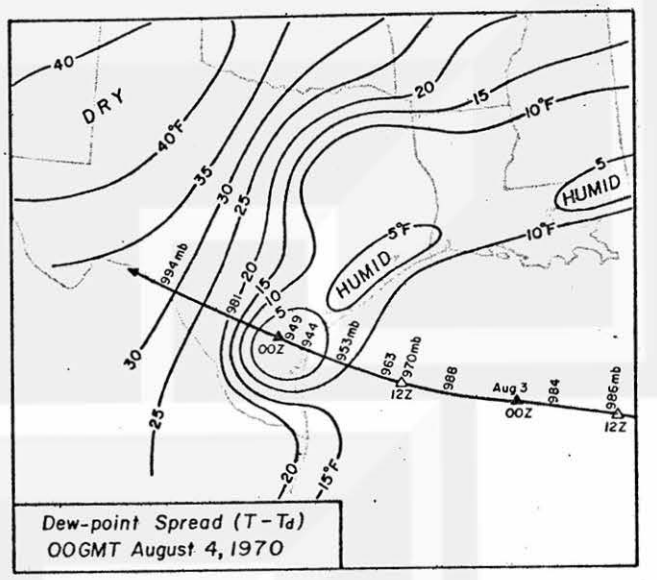

Figure 18. Dew-point temperature spread at 00 GMT on the 4th. The western eye wall began showing squall-line characteristics with thunder and downbursts.

4. HURRICANE FREDERIC (SEPTEMBER 1979)

Hurricane Frederic moved north-northeast following the east side of Camille's path 10 years earlier. Frederic was larger than Camille but its central pressure was no deeper than 943 mb (Figure 1).

During the landfall time, the diameter of the radar eye was 40 miles including the entire length of Dauphin Island inside. At Dauphin Island Sea Lab and at Dauphin Island bridge, however, the recorded windspeeds were not affected by the eye in which the windspeed is expected to decrease. For some reason, the windspeed of Frederic was probably not the highest along the eye wall.

One of the most effective means of determining the eye-wall circulation is to compute echo velocities. We have to realize that radar echoes do not move with environmental winds, however.

Figure 19 shows the radar picture at 2145 CST and echo velocities computed from successive pictures taken between 2145 and 2159 CST (14 min period). Echo movement reveals that the echo velocity along the high reflectivity ring was 80 to 85 kt while weak echoes inside the ring was as fast as 107 kt. The echo-velocity pattern suggests that the circulation center (instantaneous center of rotation) was located to the east of SY, the Ingalls Shipbuilding Yard at Pascagoula, Mississippi. The windspeed at SY began decreasing at 2138 CST when the north edge of the eye moved inland.

At 2300 CST on September 12, the weak echo region inside the eye became quite irregular. It is very difficult to determine, based on this radar picture alone, where the center of circulation is located (radar photo above). Echo velocities superimposed upon radar echoes (lower figure) shows clearly the center of circulation located inside a small echo-free hole or bay, near the northwest edge of the eye (Figure 20).

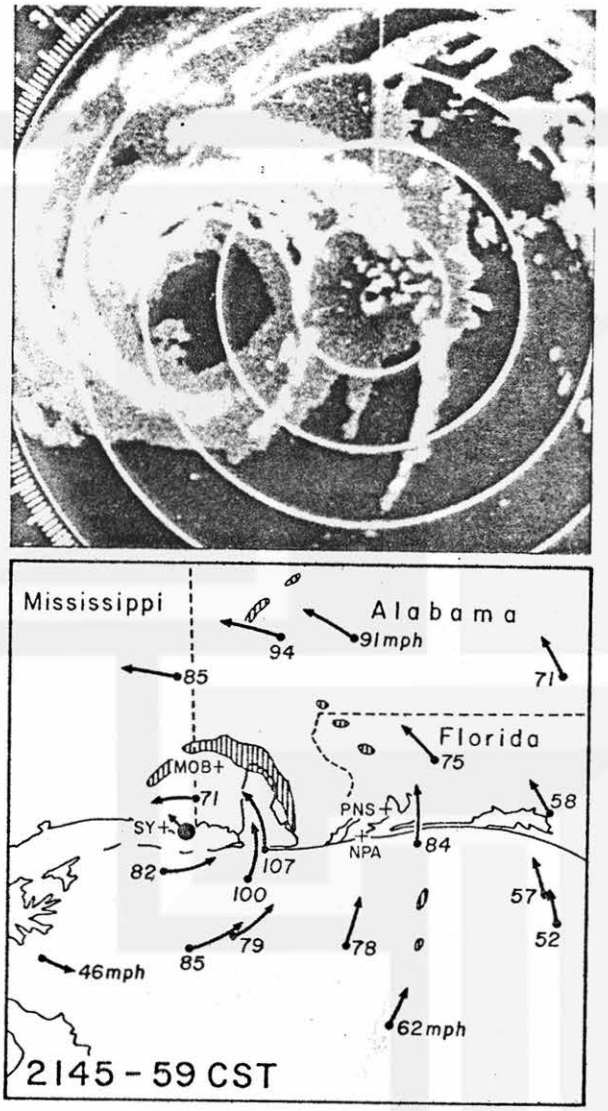

Figure 19. Radar picture from NPA taken at 2145 CST (above) and echo velocities computed from successive pictures between 2145 and 2159 CST (below).

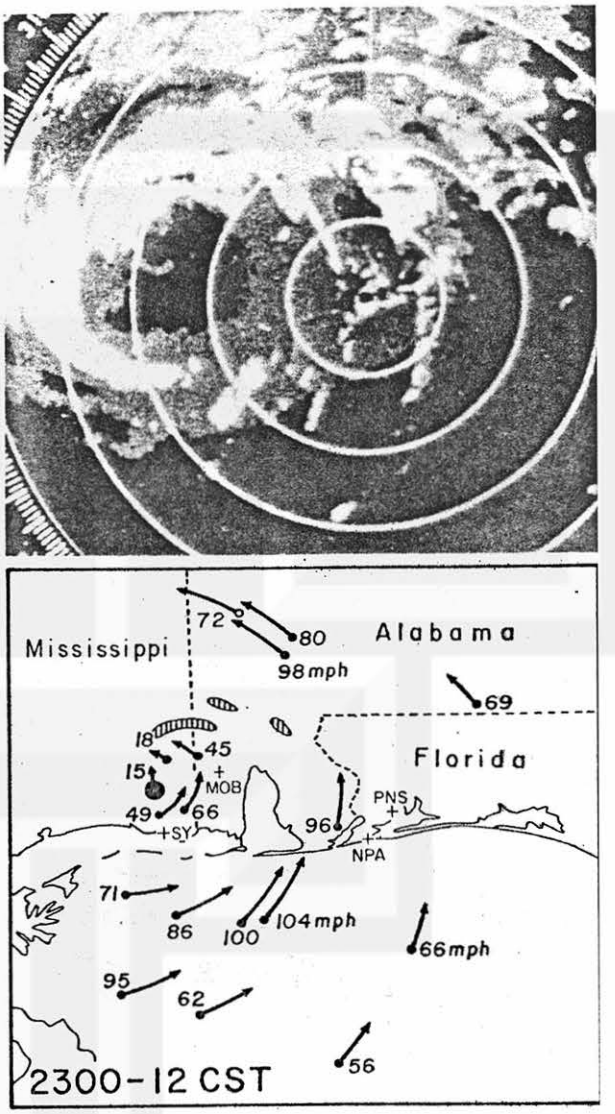

Figure 20. Radar picture from NPA taken at 2300 CST (above) and echo velocities computed from successive pictures between 2300 and 2312 CST (below). Note that the circulation center is located near the northwest edge of the echo-free eye.

These examples of radar-echo analyses present difficulties in determining the circulation center and the circle of maximum wind based on a single radar picture. Time-motion analyses, however, will add new information -- velocity vectors -- which will permit us to perform a kinematic analysis of the hurricane's motion field.

Alerted by NHEML, the University of Chicago survey team prepared to carry out an extensive aerial mapping of the Frederic damage. Two Cessna 172's were used for mapping damage vectors classified as F0, F1, and F2. The assessment methods and rules were those used currently for mapping tornado damage.

Results presented in Figure 21 reveal that damaging winds occurred on the front side of Frederic which weakened rapidly after the landfall. Just about all F2 vectors are from northeast to northerly directions with their areas limitted to within 20 miles from the coastline. Estimated 100 mph winds extended almost 100 mi inland.

There were numerous pockets and swaths of F1 (100 mph) and F2 (125 mph) winds. A close-up examination of these swaths strongly suggests that some local areas affected by high winds, 25 to 50 mph faster than those in the surrounding area.

There was a report of a tornado from Lottie in Escambria County, Alabama. Low-level traverses were made several times over the suspected tornado area. In spite of the effort in search of tornadic damage patterns, all we found was a swath of high winds across the community and nearby forest. Damage directions were divergent by 10 to 20 degrees, suggesting that the downburst winds were superimposed upon the overall hurricane circulation. Since the

Figure 21. F-scale mapping of hurricane Frederic damage based on aerial photography and mapping from a low-flying Cessna 172. Short arrow represents F0 damage, long arrow, F1, and long arrow with letter "2", F2 damage.

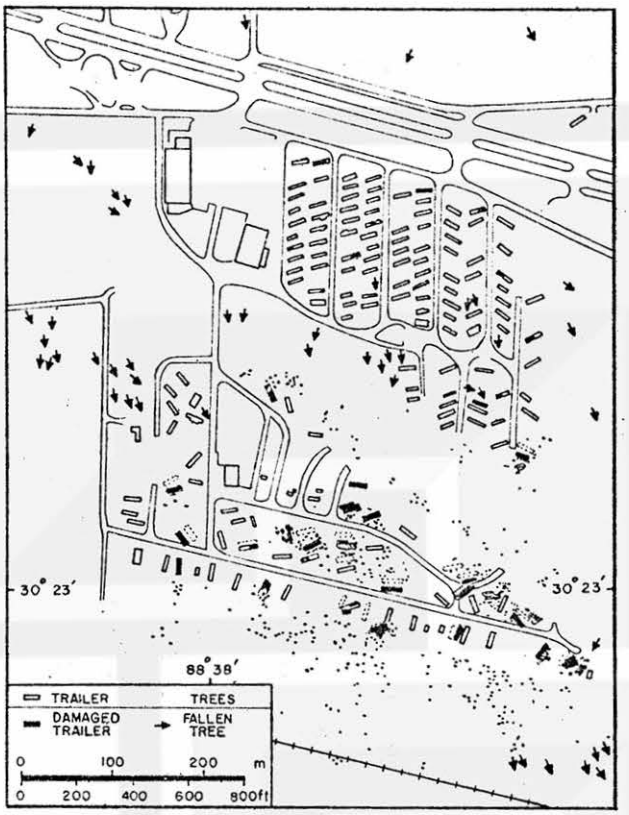

Figure 22. Shielding effects of tall pine trees which protected mobile homes in the upper-right park. The lower-left park had practically no trees and 70% of the mobile homes were damaged.

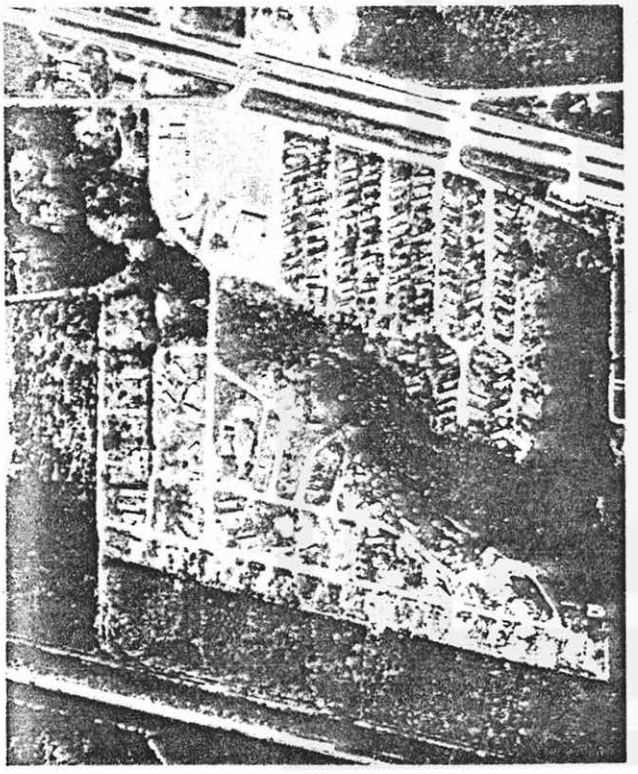

Figure 23. An aerial photograph of the mobile homes in Figure 22 (NHEML photo).

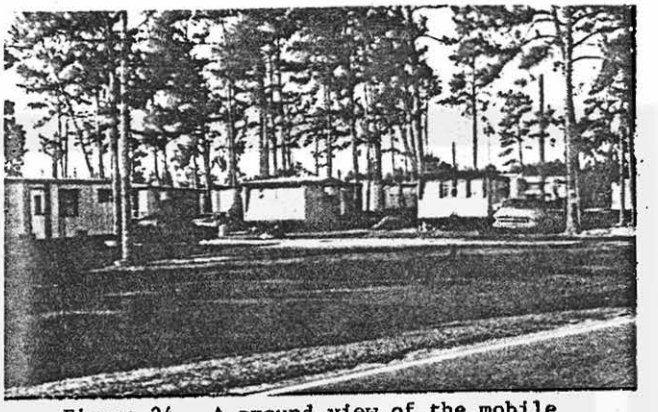

Figure 24. A ground view of the mobile homes in the upper-right park in Figures 22 and 23. These mobile homes were protected by tall pine trees.

basic hurricane winds are high, say 75 mph, an addition of 50 mph downburst winds will increase the total windspeed from 75 to 125 mph. The net wind "force" induced by the combined wind will be almost 3 times larger than the hurricane wind alone. Such an increase is large enough to let local people suspect the existence of a tornado.

The only location where a sign of tornadic wind damage was found is 8 miles southwest of Mobile Airport (MOB). A lot of pecan trees were blown down, leaving the trace of cyclonic circulation, typical of weak tornadoes.

Wind-shield effects of pine trees were observed at various locations. A most dramatic effect was seen in twin trailer parks 5 miles to the west of Pascagoula, Mississippi. Mobile homes in the northern park received practically no damage while those in the southern park were literally blown apart. The difference in the wind effect is attributed to the wind-break of tall pine trees (Figures 22, 23, and 24).

Type and age of trees, as well as the groundwater conditions, affect the ultimate damage significantly. Basic rules we found during the survey of the Frederic damage are:

1. Young pines are strong. High winds snap their trunks 5 to 10 ft above the ground.
2. Pecan trees are weak. They are uprooted easily because of their shallow roots and excessive branches.
3. Trees in river beds are weak especially when they are old.
4. Young and short trees are flexible and extremely strong. Apparently they show no sign of damage visible from the air while other trees all around are damage by estimated F2 winds.

There are also basic differences between the wind effects of hurricanes and tornadoes, especially on structures. Examination of numerous houses in Frederic revealed that extreme winds in hurricane are accompanied by "downward flow" which, in effect, pushes down the roofs of structures. Tornadic winds, on the other hand, are accompanied by an "upward current" which, in effect, pulls up roofs.

These forces, either "push down" or "pull up", are superimposed upon the aerodynamic pressure forces caused by the basic airflow impinging upon structures. The overall, definite impression, received by comparing hurricane and tornado damage, is that structures tend to withstand higher winds in hurricanes than those in tornadoes.

5. SUMMARY AND CONCLUSIONS

During the past decade, Fujita and his associates at the University of Chicago made numerous low-level flights in search of meso- and local-scale wind fields.

Three landfalling hurricanes, Camille (1969), Celia (1970), and Frederic (1979), offered golden opportunities to perform the detailed mapping of wind effects.

It has been confirmed that the local winds are superimposed upon the overall hurricane wind field. These local winds are "tornadoes" and "downbursts", and are induced by severe convective activities embedded inside the hurricane circulation.

A very basic question is the intensity and frequency of these local winds during prelanding and postlanding phases of landfall hurricanes. We know in general that tornadoes and downbursts exist in postlanding hurricanes. While over the ocean, however, confirmations of local winds can be done only by examining the low-level flight data.

Both the general public and forecasters equally want to know the exact location of hurricane's landfall as well as its mesoscale wind field. Unfortunately, not all hurricanes are alike.

Prior to landfall, hurricane Allen of 1980 was evaluated to be the worst hurricane of the century. The storm weakened prior to the landfall, and our aerial survey showed only the signs of weak winds. However, hurricane-induced tornadoes in Texas turned out to be very strong. How are they related?

It would be necessary to investigate further the structure of landfalling hurricanes from various angles in an ultimate attempt to achieve the most effective warning and evacuation of people from coastal areas to minimize casualties.

Acknowledgement

The research reported in this paper had been sponsored by NHRP, and NHRL under their grants. The current research has been supported by NHEML under grant NA80RA-C-00081.